The International Journal of Robotics Research
http://ijr.sagepub.com/

Electro-osmotic propulsion of helical nanobelt swimmers

Gilgueng Hwang, Rémy Braive, Laurent Couraud, Antonella Cavanna, Ouerghi Abdelkarim, Isabelle Robert-Philip, Alexios Beveratos, Isabelle Sagnes, Sinan Haliyo and Stéphane Régnier

The International Journal of Robotics Research 2011 30: 806
DOI: 10.1177/0278364911407231

The online version of this article can be found at:
http://ijr.sagepub.com/content/30/7/806

Published by:
SAGE
http://www.sagepublications.com

On behalf of:
ijrr

Multimedia Archives

The International Journal of
Robotics Research
30(7) 806–819

DOI: 10.1177/0278364911407231
ijr.sagepub.com

Electro-osmotic propulsion of helical nanobelt swimmers

Gilgueng Hwang[1], Rémy Braive[2], Laurent Couraud[1], Antonella Cavanna[1], Ouerghi Abdelkarim[1], Isabelle Robert-Philip[1], Alexios Beveratos[1], Isabelle Sagnes[1], Sinan Haliyo[3] and Stéphane Régnier[3]

Abstract

Micro and nanoscale mobile agents capable of self-propulsion in low Reynolds number fluids would have a great technological impact in many fields. Few known mechanisms are able to propel such devices. Here we describe helical nanobelt (HNB) swimmers actuated by an electric field-generated electro-osmotic force. These HNB swimmers are designed with a head and a tail, similar to natural micro-organisms such as bacteria and their flagella. We show that these electro-osmotic propulsion of HNB swimmers achieve speeds (24 body lengths per second), force (1.3 nN), and pressure (375.5 Pa) above those demonstrated by other artificial swimmers based on physical energy conversion. Although nature's bacteria are still more dynamic, this paper reports that the demonstrated electro-osmotic HNB microswimmers made a big step toward getting closer to their performances. Moreover, an unusual swimming behavior with discontinuous pumping propulsion, similar to jellyfish, was revealed at or above the speculated marginal limit of linear propulsion. These electro-osmosis propelled HNB swimmers might be used as biomedical carriers, wireless manipulators, and as local probes for rheological measurements.

Keywords

Biologically inspired robots, biomimetics, human-centered and life-like robotics, mechanics, design, and control, micro/nanorobots

1. Introduction

Due to recent developments in in vivo nanorobots for biomedical applications, there has been much interest in the discovery of new and efficient wireless power transfer methods and of controlled locomotion mechanisms. These kinds of novel tools would have many potential applications, such as targeting, diagnosing, and treating blood clots or cancer cells, for neural cell probing, and so on. Many approaches aim to mimic natural bacteria for the locomotion of artificial nanostructures because of their excellent motility, around 5–10 times per body size per second (Berg, 2004). Nature has adopted several different propulsion techniques. The swimming of real bacteria is mainly divided into corkscrew-type rotating propulsion and the oscillation of flagella tail (Purcell, 1977). Several studies exploring similar propulsion techniques exist in the literature, with different efficiencies. Purcell (1977) uses a definition of swimming efficiency that compares the power used to propel a body at a given velocity to the power required to simply pull the body through the fluid at the same velocity (ε = power required to simply pull the body/power consumed during propulsion). Under this definition, direct pulling with the field gradient is 100% efficient (i.e. ε=1), and other methods would always perform less. Recently, direct pulling of nanowires, nanotubes, and microtubes with excellent swimming performances (2 mm/s^{-1}, which is approximately 50–100 times per body size) were demonstrated by catalytic decomposition of hydrogen peroxide (H_2O_2). However, this technique only works in a solution, such as H_2O_2, allowing a catalytic reaction with Pt or Ag (Laocharoensuk et al., 2008; Mei et al., 2008; Sundararajan et al., 2008; Solovev et al., 2009).

[1]Laboratoire de Photonique et de Nanostructures (LPN-CNRS), France
[2]Université Paris-Diderot, France
[3]Institut des Systèmes Intelligents et de Robotique, Université Pierre et Marie Curie, France

Corresponding author:
Gilgueng Hwang, Laboratoire de Photonique et de Nanostructures (LPN-CNRS), Site Alcatel de Marcoussis, Route de Nozay, 91460 Marcoussis, France.
Email: gilgueng.hwang@lpn.cnrs.fr.

Among different propulsion methods, the use of the magnetic effect is the most widely encountered. A rotating magnetic field was used to drive the macro- and micro-scale flagella-like structure (Honda et al., 1996; Ishiyama et al., 2003; Zhang et al., 2009a). A micro bead (3 μm) was pushed for the first time by a single flagellated magnetotactic bacterium along a planned trajectory (Martel et al., 2006). Larger micro beads (10 μm) were attached to natural bacteria and moved by several bacteria flagella propulsion (Behkam and Sitti, 2006). At a 30 μm scale, bacteria flagella-like propulsion was demonstrated by an attached ferromagnetic metal pad under an external rotating magnetic field (Bell et al., 2007; Zhang et al., 2009a,b). A linear chain of colloidal magnetic particles linked by DNA (Deoxyribonucleic acid) and attached to a red blood cell can act as a flexible artificial flagellum (Dreyfus et al., 2005). Further size reduction and applying the same principle to drive artificial bacteria was achieved (Ghosh and Fischer, 2009). Lately, helical propellers have been shown to be an efficient solution at low Reynolds numbers (Abbott et al., 2009).

Concerning the driving power source, there are several limitations of using an external field. The magnetic field gradient rapidly decreases with the distance from the source. Therefore, although the helical morphology is advantageous at low Reynolds numbers by reducing the viscous drag, the swimming performance of artificial structures is still much lower than natural bacteria. To improve the swimming performance, increasing field intensity would be necessary.

However, the major challenge toward potential in vivo biomedical applications is the lack of closed-loop motion control, either by teleoperation or autonomous navigation. This lack is related to position tracking issues. Widely used non-invasive biomedical sensors or imaging devices include radiography, computed tomography (CT), ultrasound echography, and magnetic resonance imaging (MRI). Considering the real-time navigation and high spatial resolution requirements, MRI is one of the most promising solutions. Ferromagnetic objects, or even magnetotactic bacteria, were tracked and navigated under real-time MRI (Martel et al., 2009a). In the case of smaller objects at low Reynolds numbers, an additional propulsion-dedicated field gradient generator would probably be required. However, magnetic field gradient-based propulsion would be largely limited when it has to be used with an observation device, such as a MRI scanner, because of the conflict between the imaging and propelling magnetic fields. This problem can be avoided by using non-magnetic propulsion.

As a non-magnetic approach, the flapping or undulating motion of flagella was achieved in meso-scale using a commercial piezoelectric bimorph (Kosa et al., 2008). Microrobots that harness natural bacteria have also been demonstrated (Behkam and Sitti, 2006; Martel et al., 2006, Steager et al., 2007; Martel et al., 2009b). There are very few works on electric field-based wireless micro/-nanorobots. For example, diodes were actuated using electro-osmotic pumping (Chang et al., 2007a,b). It showed that the electro-osmotic field can be a good candidate for actuating micro/nanorobots. However, the work was only demonstrated in macro scale and not scaled down to micro or nano.

In this paper remote propulsion of artificial microswimmers with high dynamic mobility (5–30 body lengths per second) at low Reynolds numbers by electro-osmotic effect is described. These swimmers are based on helical nanobelt (HNB) structures. As different types of HNBs showed different swimming performances, choices of surface material and geometry are discussed along with the fabrication processes. The electro-osmotic propulsion principle and experimental setups are presented. Finally the experimental results on electro-osmotic propulsion of HNBs, with different locomotion techniques, are described.

2. Helical nanobelts as artificial swimmers

2.1. Advantages of HNBs as artificial flagella

There are several different types of bacterial locomotion, such as rotating and undulating motions. Their major features, especially in terms of surface condition, geometry, and motility, have evolved to swim efficiently at low Reynolds numbers. For example, *E. coli* flagella consist of a highly elastic body formed of protein. Therefore they can self-transform their morphology to increase their swimming velocity at low Reynolds numbers. Their filaments can exist in different polymorphic forms, having distinct values of curvatures and twist. These polymorphic transformations can result in motions, such as tumbling or bundling, depending on the direction of rotation uniformity (Turner et al., 2000). It is considered that such abilities of natural bacteria are mainly attributed to the non-linear mechanics of their flagella. Concerning the hydrodynamic motions, it is necessary to have a corkscrew motion to swim at low Reynolds numbers (Purcell, 1977). The motion is inspired by biology (e.g. nature's bacteria flagella propulsion of *E. coli*). Purcell (1977) mentions only the hydrodynamic point of view; however, in reality, nature's bacteria swim mainly powered by chemical energy (e.g. chemotaxy) from nutrient sources inside bodily fluid. The highly motile swimming behavior of nature's bacteria is mainly due to such efficient chemical energy conversion mechanism from the environment. They do this process with a large surface-to-volume ratio to increase such effect. That is one of the reasons why flagella exist, although they increase viscous drag; they also need to rotate to reduce this drag.

However in engineering, the surface electro-kinetic effect should also be considered. The major challenge in mimicking nature's bacteria is to develop a similarly efficient surface electro-kinetic effect with a varying mechanical property to adapt the motion to a harsh environment.

To mimic similar performances of natural bacteria, ultra-flexible nanostructures with large non-constant mechanics are considered necessary. The mechanical durability is also an important issue, especially in harsh environments. Therefore, we develop HNBs to form microswimmers to mimic these two major features. Firstly, compared to the nanorods or tubes, HNBs have a higher surface-to-volume ratio, larger range mechanics (Acosta et al., 2011), and higher piezoresistivity (Hwang et al., 2009). Concerning hydrodynamics, straight nanobelts undergo less viscous drag if we assume that the structures are rigid, meaning there are no deformations during their propulsions. It should be noted that the proposed work does not aim to design swimmers that have efficient hydrodynamics, but to improve their electro-kinetic effects. Actually the demonstrated high performance of HNB swimmers is attributed to the spring-like propulsion generated by the viscous drag. Therefore in this aspect, helical morphology is advantageous compared to other-shaped nanostructures. Concerning the surface electro-kinetic effect of bacteria, their propulsions are enhanced by propelling flagella motions to reduce the viscous drag. We aim to mimic such surface electro-kinetic effect of bacteria flagella. Therefore, we create a helical-shaped device with high surface-to-volume ratio, mimicking the flagella, to reduce the viscous drag by creating spring-like propulsion and liquid slip via local electro-osmotic flow (EOF) around the surface of swimmers. HNBs are one of the most flexible nanostructures that can be fabricated using standard microfabrication techniques with controlled geometry. Helical morphology appears as an adapted solution for electro-osmotic propulsion because of the large surface-to-volume ratio to maximize the external energy reception. Another advantage is their elasticity to passively self-adapt their morphology in thick liquid environments by reducing viscous drag. Different types of nanobelts were synthesized and mechanically characterized (Bell et al., 2006; Gao et al., 2006). Recently, HNBs were revealed to have very large non-linear mechanical properties along with giant piezoresistivity (Hwang et al., 2009). This giant piezoresistivity was partly due to the piezoelectric charges induced by stress gradients. In the case of electro-osmotic propulsion, different surface coatings with thin films can also be achieved by standard microfabrication techniques to improve electro-kinetic energy. The high surface-to-volume ratio of HNBs can disadvantageously increase friction at the liquid/solid interface. HNBs with hydrophobic surface coatings can reduce this friction to improve the swimming performance.

In addition, harvesting energy from the environment would be an important advantage for mobile micro/nano agents. Piezoelectric nanogenerators based on zinc oxide nanowire arrays were firstly proposed by Wang and Song (2006). A nanowire-based, self-powered nanosensor has also been demonstrated (Xu et al., 2010). When the HNBs swim at low Reynolds numbers, viscous drag can cause repeated passive motions, such as compressions and elongations. This can induce piezoelectric charge onto the surface of HNBs, which results in the increase of zeta potential. The increased zeta potential improves the swimming performance of HNBs. Therefore, the repeated passive motions of HNBs during their swimming at low Reynolds numbers can self-harvest electro-kinetic energy due to their giant piezoresistivity (Hwang et al., 2009).

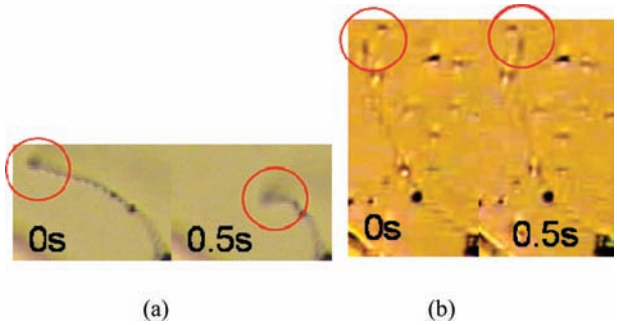

Fig. 1. Oscillation in 1 Hz of helical nanobelts (HNBs) with hydrophobic and hydrophilic surfaces: (a) 1 Hz oscillation of hydrophobic HNB; (b) 1 Hz oscillation of hydrophilic HNB.

Therefore, considering the limitations of conventional propulsion mechanisms, the remotely powered gradient pulling of HNBs should be efficient to swim in a low Reynolds number liquid environment (Abbott et al., 2009).

2.2. *Fabrication process*

The geometrical parameters of the helix, such as diameter, chirality, helicity angle, and pitch, were precisely controlled (Zhang et al., 2005; Bell et al., 2006). In this paper, the process was extended with different materials, such as metals, dielectrics, and polymers. Four different types of HNB-based nano-swimmers, varying the materials and geometries (summarized in Table 1) are produced for testing purposes. Their propulsion efficiency is then compared in electro-osmotic propulsion experiments and in fluid dynamic simulations.

Figure 2 illustrates the fabrication process. The initial layers were grown on semi-insulating GaAs wafers (AXT Inc. wafers) using a molecular beam epitaxy system (VEECO, Gen II MBE) equipped with a valved cracker for As and solid sources for Ga and In (Figure 2(a)). For *n*-type doping, a Si source was used. Substrate temperature was measured by a pyrometer. After a thin GaAs buffer layer, the 500 nm thick sacrificial AlGaAs layer is deposited. The layer contains 20% Ga in order to prevent oxidation. The sacrificial layer in previous designs was made of AlAs. The oxidation of these layers after exposure damaged the InGaAs/GaAs bilayer. On top of the sacrificial layer the InGaAs/GaAs layer is deposited, which later self-forms into a nanospring. An In content of 15% in the InGaAs layer was determined by X-ray diffraction (XRD) measurements. The thickness of this layer must be smaller than the critical

Table 1. Specifications of different types of artificial bacteria (helical nanobelt (HNB))

	HNB1 low	**HNB2 high**	**HNB3 Cr/Ni**	**HNB4 photoresist**
Thickness $In_0.15Ga_0.85As/GaAs$ (nm)	11.6/15.6	8–10/15.6	11.6/15.6	
Thickness Cr/Ni or photoresist (nm)	NA		Cr/Ni 10/10	Photoresist 50
Diameter (tail=head), pitch & width (tail) (μm)	2.1, 14, & 2.5			
Number of turns (tail)	4.5 turns			
Length (head/total) (μm)	12/74			
InGaAs/GaAs doping (N_D)	4.4×10^{18} cm^{-3}	8.5×10^{18} cm^{-3}		

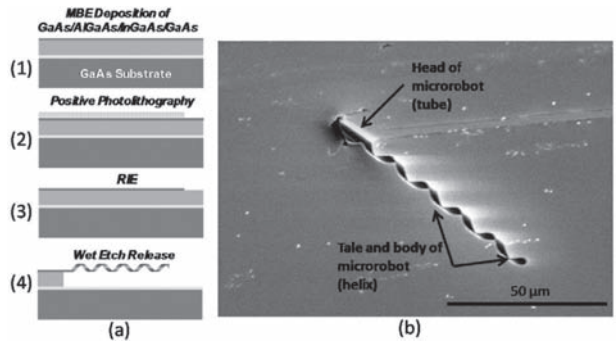

Fig. 2. Basic fabrication process sequence of a helical nanobelt (HNB). (a) (1-4) Initial planar bilayer, patterned through conventional microfabrication techniques folds itself into a three-dimensional nanostructure during wet etch release. (b) Produced HNB with a tail and a head (scanning electron microscopy photo).

thickness in order to maintain elastic strain. The layer properties, along with other specifications of the structures, are summarized in Table 1.

During the deposition of the InGaAs/GaAs bilayer on this wafer for HNB1, we attempted to get a slightly lower doping concentration on the wafer than was used for HNBs 2–4. From the results it seems that the doping concentration was too high, which resulted in a partial self-compensation and, therefore, in a decrease in the effective doping concentration. The doping concentrations of the structures are 4.4×10^{18}cm^{-3} and 8.5×10^{18}cm^{-3}. The initial pattern can be created through photolithography. Reversible photoresist AZ5214 was used as a resist. After the development of the resist, reactive ion etching (RIE) with a SiCl4 gas was used to transfer the pattern to the InGaAs/GaAs bilayers (Varoutsis et al., 2005). For HNB4, the thickness of the photoresist was reduced to around 50 nm with O2 plasmas. For metallic HNB3, the Cr/Ni layers on the surface and on the heads to which the structures are fixed at the end were created before RIE through a lift-off process with negative photoresist AZ5214.

The Cr layer is 10 nm thick and serves as an adhesion layer. The 10 nm thick Ni layer is used for metal HNB3. Finally, a 2% HF aqueous solution at 4°C was used to selectively etch the AlGaAs sacrificial layer under the InGaAs/GaAs heterostructures for the self-forming of the nanostructures (Figure 2(a)). During this wet etch, the patterned bilayer curled up along a ⟨100⟩ direction releasing the internal strain and forming three-dimensional (3D) structures. The direction of the scrolling is determined by the anisotropy in stiffness of the InGaAs/GaAs bilayer. After the wet etch release, the chips were rinsed in deionized water and subsequently in isopropyl alcohol (Hwang et al., 2009). Samples are also conserved in isopropyl alcohol in order to prevent oxidation by watering of the heads to which the structures are fixed.

3. Electro-osmotic force propulsion

3.1. Principle of HNB electro-osmotic propulsion

The propulsion of HNBs involves two conversions: transforming energy from an external source to a force, and transforming this force into a motion. The proposed method to supply power remotely to HNBs is an electro-kinetic process. Its main advantages for in vivo applications are the good tolerance of living organisms to electric fields and its compatibility with medical MRI.

In general, the surface charge that develops at the solid–liquid interfaces plays an important role in a number of electro-kinetic processes. Owing to the presence of a thin interfacial layer named the Stern layer, it results in a non-zero electric potential at the liquid interface, also known as the zeta potential ζ. This potential is screened by mobile counter-ions diffusing in the liquid in a layer generally named the Electrical Diffuse Layer (EDL), which has a typical thickness of a few tens of nanometers depending on the solution ionic strength. Under an electric potential difference, the resulting electric field puts in motion the excess counter-ions in the EDL. This moving layer drags the whole liquid inside the fluidic medium, resulting in 'plug-like' flows, also referred to as EOFs. In addition, one should also consider the surface charge developing at the HNB surface. In the case of a HNB floating in liquid, its own Stern layer generates a flow that applies a hydrodynamic pressure on the surface of the robot, propelling it in the opposite direction.

Figure 3 depicts the electro-osmotic propulsion mechanism through the interface between HNB's thin membrane surface and liquid medium solution. Since the propulsion

force occurs through the whole surface, the large surface-to-volume ratio of HNBs is very advantageous. Figure 3 is a schematic diagram to show the propulsion principle. It should be noted that the polarity in the figure is not specific for all cases with various materials, but is a positively charged example to explain the principle. EOF is generated by the external electric field on net mobile charges in liquid medium. The chemical equilibrium at the solid and liquid interface makes an interface acquiring a net fixed electrical charge. Nearly all materials acquire surface charge in water, more often negative but sometimes positive. It depends on the surface material and liquid electrolyte. For example, in our case, *n*-type GaAs and the metallic surface could be charged positively in water or any equivalent. In addition, the glass substrate or dielectric materials are negatively charged in the same medium. If the solid is positively charged, the mobile electrons are attracted near it in the liquid. Then a mobile ion layer (Debye layer) forms near the surface. When an electric field is applied, the ions in the Debye layer move (the flow is the EOF). Potential generated at the interface is zeta potential. The flow speed is the function of zeta potential. The zeta potential depends on the materials of surface. Finally the propulsion is made by two effects: a direct pulling by electrophoretic force of the HNB and also the channel surface and HNB surface flow motion driven by electro-osmotic force, as shown in Equation (2). Quantifying the contributions of EOF depends on the distance of the HNB to the channel surface, because the EOF is the function of the cross-section of channel. In the demonstrated configuration of the HNB and the surface, the electrophoretic force and EOF of the channel surface dominate, as they have the same propulsion direction. The local EOF generated around the surface of the HNB makes the liquid slip out of the HNB in the opposite direction to propulsion; thus, it further increases the forward-propelling force.

HNBs' motility results from a local electro-osmotic flux powered by an external field. The specific direction of HNBs' propulsion along the cathode and anode probes indicates that a direct current (DC) field gradient along the HNB is responsible for this propulsion. The equivalent circuit can predict that the electro-osmotic propulsion force is affected by the difference of electrical resistivity between the medium solution and the HNB (Figure 3). The electric voltage applied to the HNB by the external field can be estimated from a serially connected resistor model describing the ionic conductance through the liquid medium, and the capacitors for the ionic layers. In a DC electric field, the resistance is the leading contribution. The resulting DC voltage of magnitude V_d induced in the HNB is modeled as

$$V_d = \frac{R_2}{R_1 + R_2 + R_3} V_{\text{ext}} \tag{1}$$

where V_{ext} is the DC input voltage applied to the probes in the Petri dish and R_1 (resistance between the left-hand electrode and the HNB), R_2 (resistance of the HNB), and R_3 (resistance between the HNB and the right-hand electrode) are depicted in Figure 3. Assuming that the resistance of the liquid is linearly proportional to the distance between the probes, Equation (1) can be simplified as $V_d = E_{\text{ext}}\, l_d$, where l_d is the length of the HNB body and E_{ext} is the external DC field. The external DC field between the electrodes makes electro-osmotic fluid flow along the HNB body.

Considering a liquid electrolyte, consisting of positive and negative particles in liquid solution, the interface between the electrolyte and the container wall generally forms a double layer in equilibrium, where a non-zero surface charge is screened by a very thin diffuse layer of excess ionic charge of width λ, the Debye screening length (typically 1–100 nm). The double layer is effectively a capacitor skin at the interface, which has a small voltage ζ across called the zeta potential. The effect on the HNB and also the environment under the electric field is further detailed in the following model, which decomposes the part of intrinsic electrophoretic force directly generated to the HNB and the EOF from the surface interaction. Considering a tangential electric field E_{ii} applied in parallel to a flat surface, the electric field acts on ions in the diffuse part of the double layer, which drag the fluid to produce an effective slip velocity outside the double layer by the Helmholtz–Smoluchowski formula (Equation (2)) (Hunter, 2001):

$$u_{11} = \left(\frac{2\varepsilon_0 \varepsilon_r \zeta_{\text{HNB}} H}{3\eta} - \frac{\varepsilon_0 \varepsilon_r \zeta}{\eta} \right) \vec{E} \tag{2}$$

where $\varepsilon_0 \varepsilon_r$ and η are the electrolyte permittivity and fluid viscosity, respectively, which are constants (environment parameters). Increasing the speed of the HNB requires increasing ζ_{HNB} and H, which are the zeta potential around the surface of the HNB and the Henri function, which depends on the geometry and hydrodynamic properties and the external field (E). On the negative term of the equation, the Zeta potential ζ on the borders of the surface is inversely proportional to the resulting speed, thus it should be minimized and controlled by applying experiments under a closed microfluidic channel.

An important application of EOF is capillary electro-osmosis, where an electric field is applied down a capillary tube to generate a uniform plug flow (Equation (2)), driven by the slip at the surface. Typical flow speeds of 100 μm/s are produced by a field of 10 V/mm. This value will be used to compare the swimming performance of HNBs. It should be noted here that the electro-osmotic propulsion does not depend on the size of the micro-agents. Thus, a microscopic HNB could move theoretically about as fast as a macro-sized one.

3.2. Electro-osmotic propulsion experimental setup

HNBs are detached from the substrate by micromanipulation. At the start of the experiments, the fixed end of the produced HNBs are cut and released from chips using

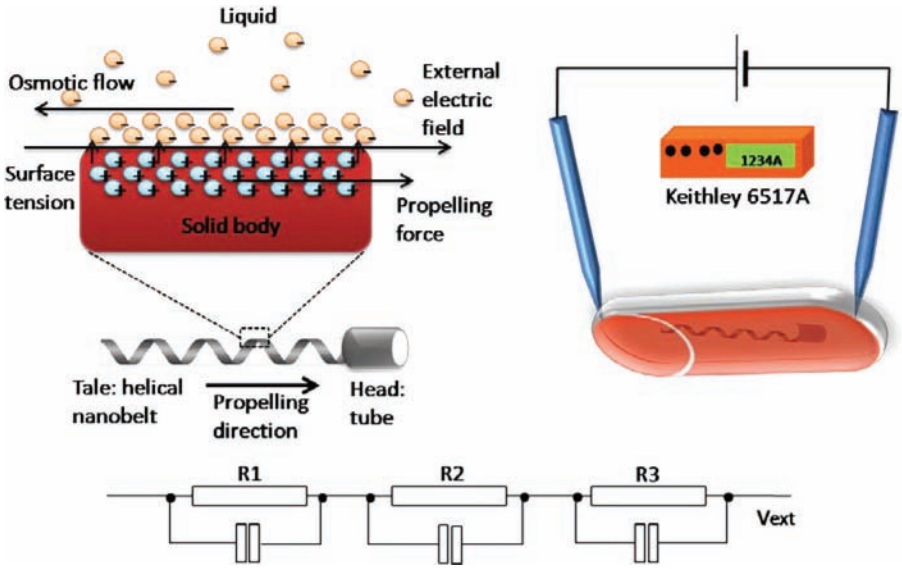

Fig. 3. Schematic diagrams of the experiments for helical nanobelt (HNB) swimming. A direct current bias was applied between two electrodes located through the axial direction of the HNB body. Thus the propulsion direction can be controlled and predicted by the configuration of electrodes. For controlling the direction of the electric field, micromanipulators with tungsten probes were utilized to form electrodes.

a setup with two probes with high positioning accuracy under an optical microscope. The same probes are also used to generate the electric field through the liquid medium and HNBs. The complete experimental setup is shown in Figure 4. Two nanorobotic manipulators (Kleindiek, MM3A) are installed under an optical microscope; each has three degrees of freedom, and respectively 5, 3.5, and 0.25 nm resolutions in the *X*, *Y*, and *Z* directions. For the application of the electrical field and high-resistance measurement, an electrometer with a DC power supply (Keithley 6517A) is used. Two probes attached to each side of manipulators are positioned within less than 1 mm. To avoid optical reflection from the meniscus between the probes and the liquid medium interface, longer probes (∼5 mm) with sharp tips (diameter around 100 nm) are used.

4. Electro-osmotic propulsion experiment

4.1. Propulsion experiment with an electro-osmotic pump

Figure 5(a) describes the series of photos taken from the recorded video and the tracked HNBs' trajectories in forward propulsion. An external DC field of 118 V/mm was applied for the forward propulsion and results in backward motion in negative potential.[1] The velocity achieved with this field and configuration is 126 μm/s, which exceeds the velocity of *E. coli* bacteria with a rotating frequency of 100 Hz (Berg and Brown, 1972; Berg, 2004). Since the sizes of HNBs and natural bacteria (e.g. *E. coli* bacteria) are different (HNB is 10 times larger than *E. coli*), relative velocities were compared using units of body length.

In experiments with an electric field of 239 V/mm, a velocity of 1785 μm/s is achieved, corresponding to 24 body lengths per second. It should be noted that *E. coli* bacteria moves at approximately 10 body lengths per second (Berg, 2004).

4.2. Controlled swimming experiments of HNBs

Figure 5 demonstrates the forward and rotating propulsion of HNBs. Experiments are depicted in Figures 5(b) and (e). The swimming propulsions of HNBs are achieved by modifying the electrodes' configuration. A series of snap shots during forward (Figure 5(a)) and rotating (Figure 5(d)) propulsions were taken during the propulsion experiments. The trajectories of each swimming experiment are displayed in Figures 5(c) and (f). For the trajectories, video analysis software and a custom-made C++ program are utilized. Rotation of HNBs was achieved by their aligning them to the applied field direction. The probes attached to manipulators can change the configuration to generate the desired electric field gradient. Please note that in this case the rotation was achieved using a HNB fixed in one extremity while the other was free. The electrode configuration was fixed to make the HNB rotate. Furthermore, the forward and backward swimming direction can be converted without the complicated tumbling motion of *E. coli* bacteria.[1]

It is confirmed that HNBs' swimming directions could be easily controlled by differentiating the field gradient. For the steering control, the field gradient needs to be aligned to the rotational axes of the HNBs. In the case of an untethered

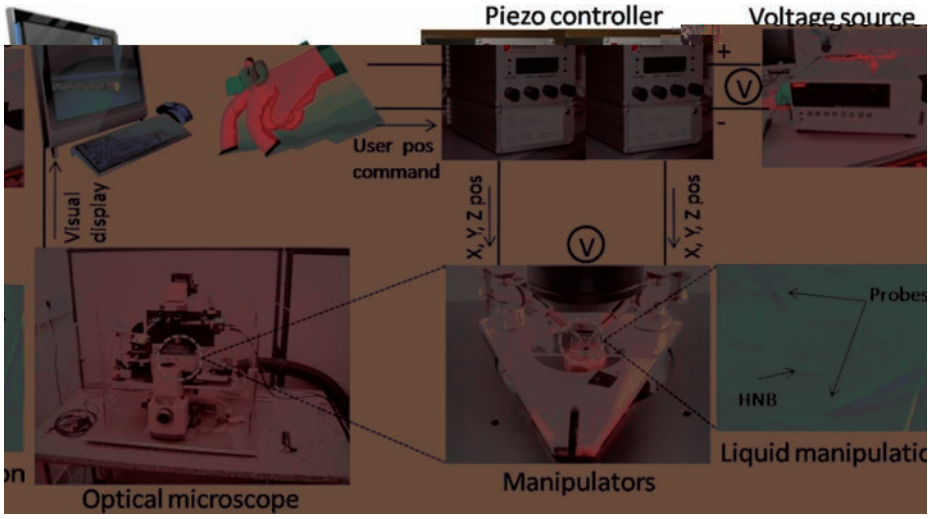

Fig. 4. System setup for electro-osmotic propulsion experiments. An optical microscope with a camera is used to give user visual feedback and thus proper manipulation in liquid. The user operates the piezo controller to manipulate tungsten probes, which are used to manipulate helical nanobelts and to apply the electric field generated by an external voltage source.

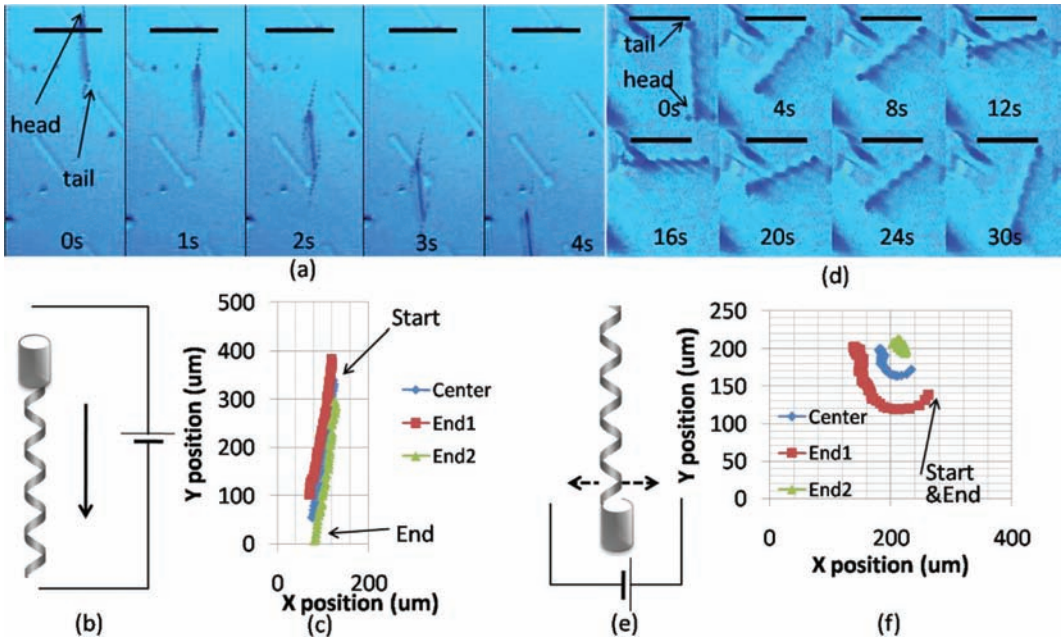

Fig. 5. Different swimming propulsions of helical nanobelts are achieved by modifying the electrode configuration. A series of snap shots during backward (a) and rotating (d) propulsions are taken during the experiments ((b) and (e)). The trajectories of each swimming experiment are displayed in (c) and (f). The scale bars in (a) and (d) are respectively 80 and 60 μm.

HNB, the rotation is achieved by controlling the field gradient (see Extension 2).The high surface-to-volume ratio of HNBs increases the swimming efficiency by increasing the charged area in a given volume and mass.

The maneuverability of the currently demonstrated electro-osmotic HNBs is still limited to the basic motions compared to the magnetic field-based approaches. However, this issue can be addressed using an array of embedded electrodes.

4.3. *Estimation of the propulsion force*

The force generated by the HNB's swimming is estimated from the drag it overcomes, considering its shape approximately as an ellipsoid (Ghosh and Fischer, 2009):

$$F = \frac{4\eta\pi a v}{\left[\ln\left(\frac{2a}{b}\right) - \frac{1}{2}\right]} \tag{3}$$

where a and b are the dimensions along the longitudinal and lateral axes respectively, η is the viscosity of the liquid medium, and v is the speed of the HNB. For a 74 μm long HNB with a diameter of 2.1 μm moving at 1.8 mm/s in isopropyl alcohol medium, the generated force of 1.3 nN (Equation (3)) is an order of magnitude higher than the conventional optical trap force, which is less than 200 pN. Furthermore, HNBs can apply a large pressure, up to 375.5 Pa, which can be advantageous for local manipulation, such as on biological membranes (Park et al., 2007; Little et al., 2008).

4.4. Unusual swimming behavior of HNBs

The swimming performances of different HNBs are analyzed as a function of the parameters controlling the electro-osmotic propulsion force. The maximum velocity of a HNB in isopropyl alcohol medium as a function of electric field intensity is characterized in Figure 6. A 74 μm long HNB is used for the tests. The intensity of the field is increased from 24.99 to 239.66 V/mm. The maximum velocity was not linearly proportional to the applied field intensity, especially at higher field intensities above 87.75 V/mm. This can be explained by the fact that HNBs swimming in isopropyl medium have relatively higher Reynolds numbers in this region compared to the water. The Reynolds number can be calculated by the following equation (Berg, 2004):

$$Re = \frac{Lv\rho}{\mu} \tag{4}$$

where L is the length of the HNB, v is the velocity, ρ is the density of the liquid, and μ is the viscosity of the liquid. For isopropyl alcohol, the kinematic viscosity (μ/ρ) is approximately 3.6×10^{-2} cm^2/s; thus, the Reynolds number is proportional to the length and velocity of the HNB. In natural bacterial propulsion with 1 μm length and a velocity of 30 μm/s, the Reynolds number is 3×10^{-5} in water. For example, a 74 μm long HNB swimming at 1785 μm/s in isopropyl alcohol medium has a Reynolds number of 3.6 $\times 10^{-2}$, which is much higher than bacterial propulsion. It involves more inertial effect during the propulsion and may explain the non-linearity of the velocity versus electric field. In our experiments, the swimming velocity of HNBs is between 4.4 and 1785 μm/s. The Reynolds numbers are thus between 3.3×10^{-4} and 3.6×10^{-2}. It is apparent that the linear relation between the field intensity and the velocity is achieved with a velocity less than 87.75 V/mm and Reynolds numbers around 4.3×10^{-3}. All other previous bacteria-like propulsions demonstrated within this velocity are around 200 μm/s (Abbott et al. 2009; Zhang et al. 2009a,b). This number could be at the marginal limit representing natural bacterial propulsion. The unusually fast-swimming propulsion demonstrated in this work is due to the generated inertial force overcoming the viscous drag by reaching higher Reynolds numbers. The inertial effect of a rigid-body swimmer at a low Reynolds number is negligible. According to the speculation based on empirical experiments, HNBs (the stiffness of HNBs at neutral position can be around 0.001 and 0.00001 N/m in longitudinal and bending, respectively) can reduce the viscous drag by passive motions, such as oscillation, rotation, and compression, due to extreme elasticity. As a matter of fact, the HNB continues to swim for a while even though the field is cut off when it is accelerated to a velocity faster than the critical velocity.

In order to understand this unique swimming behavior of HNBs, the swimming propulsion of HNBs is analyzed in further detail. The captured images of swimming propulsion of HNBs from a high-speed Dalsa Genie Complementary Metal Oxide Semiconductor (CMOS) camera (300 × 300 pixels, 342 fps) reveals that HNBs swim like jellyfish by a non-continuous (pumping and propulsion) swimming motion (Figure 7 and see Extension 3). In this case, they were accelerated with an electric field of 115 V/mm in order to undergo the inertial effect. This iterative passive deformation can reduce the viscous drag, and also generate the surface charges of HNBs to enhance local electro-osmotic force, due to their piezoresistive charge accumulation (Hwang et al., 2009). Therefore, the created surface charges increase the induced local electro-osmotic force and thus could contribute to the non-linear curve of the maximum velocity. This self-generated power could enable the HNBs to continue their swimming even after the external field is cut off. Hence, it appears that HNBs can also operate as highly dynamic actuator elements.

Furthermore, the non-linearity and fluctuations of the curve in Figure 6 are also attributed to intermolecular interactions of the HNB with the substrate. In particular, the heavier tube-type heads of HNBs were apt to submerge more than the body and tail, which makes the initial energy to break this interaction difficult to predict.

Finite element simulations in liquid medium were performed to estimate the flow around the unusually fast-swimming HNBs. Figure 8(a) shows the cross-sectional view of the HNB moving with a velocity of 1 mm/s. Although the inside of the HNB is slightly undulated, a very regular laminar flow was estimated around it. As was expected, the flow speed was slower inside the HNB and was faster outside. This laminar flow is due to the helical morphology with the ultra-thin layers of the HNB, even though the flow speed was fast for the given dimensions. The Reynolds number was around 10^{-2}, resulting in a very viscous behavior. To further estimate the undulation inside the HNB, a 3D model of a HNB was created from the assembled hexahedral blocks (Figure 8(b)). This coarse model reduces the calculation time of the finer model. The same phenomenon, with a very much slower laminar flow inside and a faster one outside the HNB, is observed. In this case, the flow inside the HNB was winded slowly. This reveals that the fast-swimming HNB can generate inner torque, and thus rotates

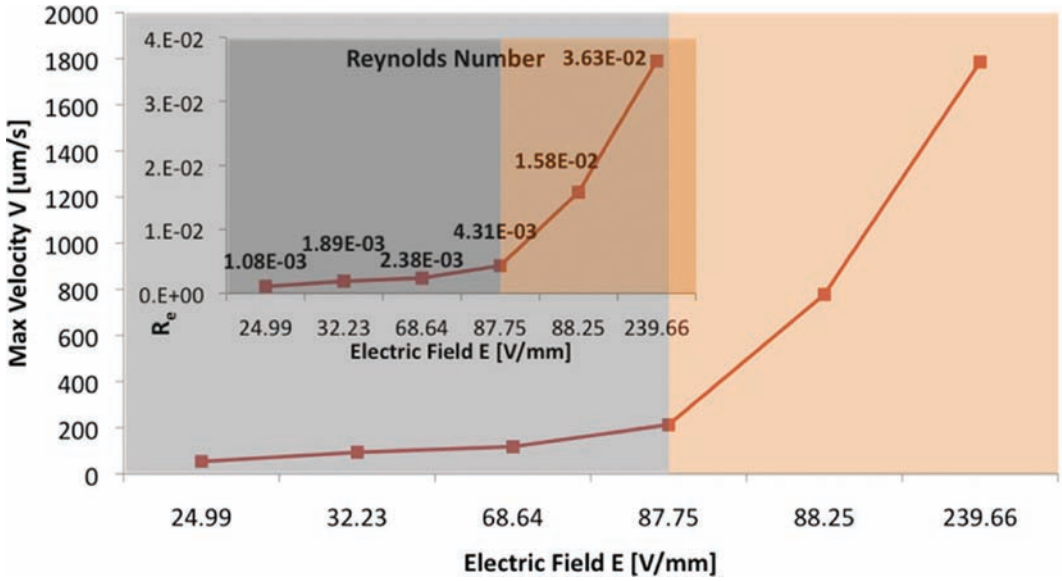

Fig. 6. Dependence of helical nanobelt (HNB) velocity on applied electric field intensity. The plot was obtained during the swimming experiments of a 74 μm long HNB in isopropyl alcohol medium. The non-linearity of the swimming performance is demonstrated in the region with electric field intensity higher than 87.75 V/mm. The inset figure shows the Reynolds numbers in different velocities versus the applied electric field.

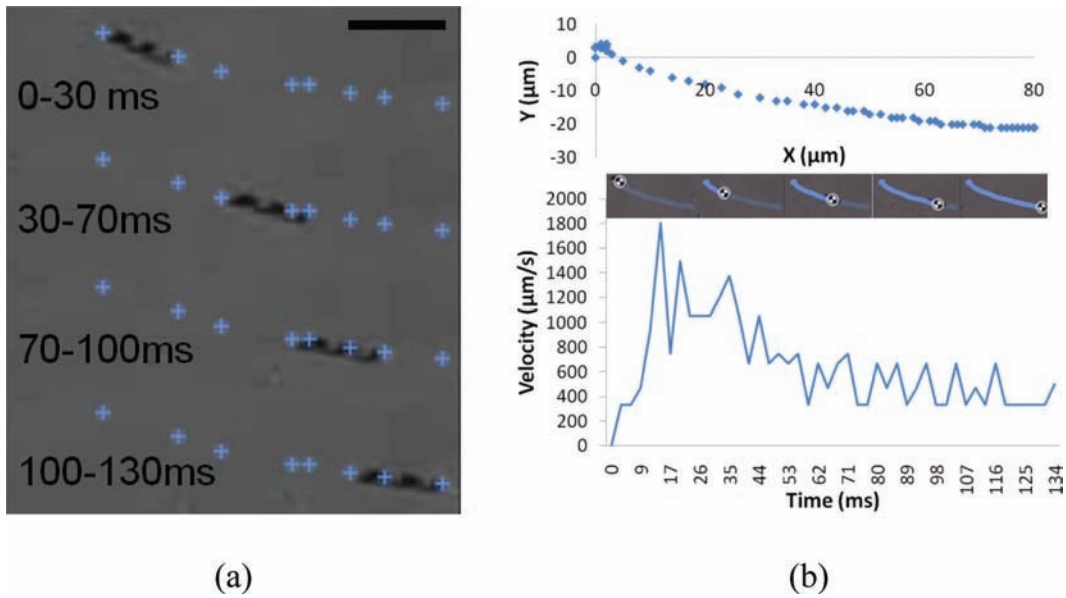

Fig. 7. Discontinuous swimming propulsion of the helical nanobelt (HNB) from high-speed camera analyses (342 fps): (a) captured images of the HNB at each discontinuous motion; (b) visually tracked trajectory of the HNB motion in the x-y plane and non-constant velocity. The scale bar in (a) is 30 μm.

the structure to balance the energy. This behavior is also observed experimentally and is depicted in Extension 4. The rotation energy contributes to keep the flow around the HNB very laminar while it swims very fast. Therefore, it is predicted that swimming performance would highly depend on the surface geometry, especially inside the HNB.

5. Swimming performance characterizations

5.1. HNBs with different zeta potentials

To further understand the repeatable swimming behaviors due to an electro-osmotic force and to find the optimized design parameters, especially the surface profile, the swimming performances of four different types of HNBs

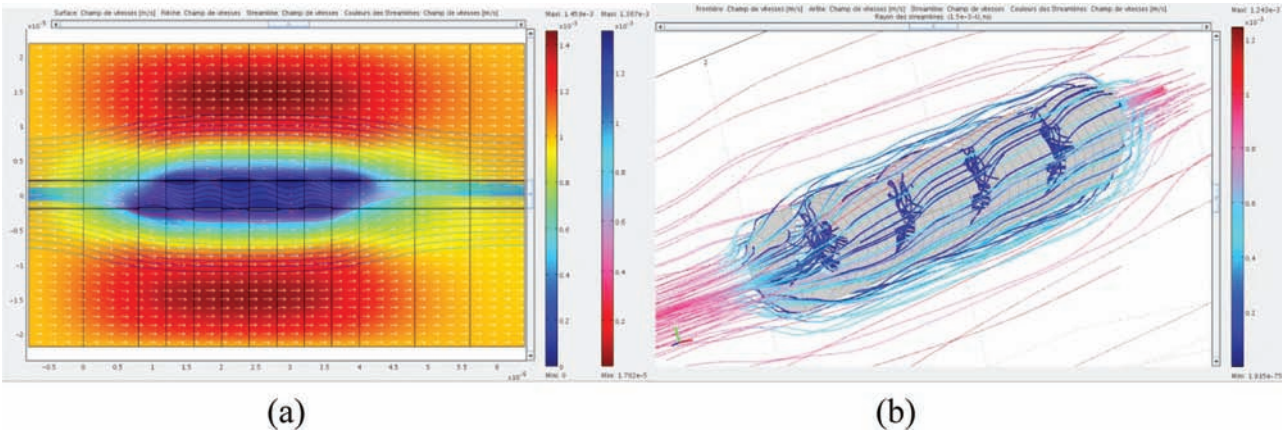

Fig. 8. Hydrodynamic simulations using finite element modeling: (a) two-dimensional stream around the helical nanobelt (HNB); (b) coarse three-dimensional model around the HNB.

were characterized. High and low-doping HNBs, a metallic (Cr/Ni) one, and a dielectric counterpart were analyzed. Figure 9 shows the average and maximum propulsion velocity and acceleration normalized by the applied electric field. HNB performance was investigated in several steps (6–11 steps) ranging from 24 to 401 V/m. It was difficult to compare the four HNBs in identical single field intensity, because the experimental configuration of probes and HNBs are difficult to maintain in between each experiment. Therefore, a statistical average velocity was chosen to describe the general behavior of each different HNB. It should also be noted that experiments on different types of HNBs were conducted on different days, which might slightly change the electrical resistivity of the liquid medium. Even though the exact resistance values of the utilized HNBs were not verified because of the difficulty in collecting them after experiments, the intrinsic resistance of the HNBs can be predicted as $R_{\mathrm{HNB4}} > R_{\mathrm{HNB1}} > R_{\mathrm{HNB2}} > R_{\mathrm{HNB3}}$. Hence, the average and maximum velocities and accelerations depend on the resistance of each HNB, as was expected from Equation (1). Highly doped HNB2 showed better swimming performance than low-doped HNB1. This can be explained by the fact that the InGaAs layer thickness (estimated as 8–10 nm) of HNB2 is slightly thinner than the one of HNB1 (11 nm). It results in better performance in HNB2 than HNB1 from the reduced gravity effect and hydrodynamic friction, regardless of the higher conductivity. It reveals that the doping concentration does not play a major role in the swimming performance compared to the geometry or volume effect. It should also be noted that HNB3 and HNB4 are slightly thicker than HNB1 and HNB2 because of additional metallic or dielectric layers (Cr/Ni 10/10 nm, AZ5214 photoresist around 50 nm, Table 1).

However, HNB3 had lower performance, while HNB4 was better than the others. In the case of HNB3, this can be explained by the increase in hydrodynamic friction during swimming, which slows down the HNB. Furthermore,

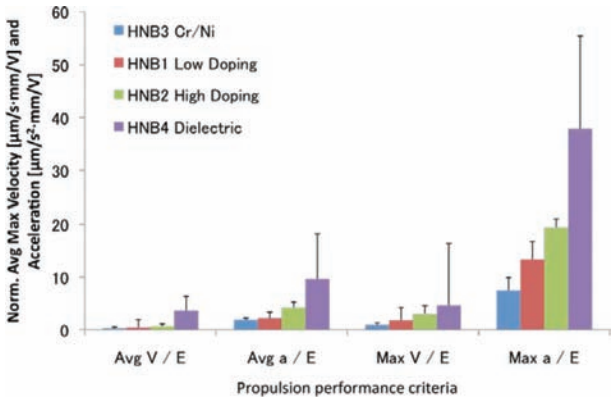

Fig. 9. Dependence of normalized velocity and acceleration of propulsion on four types of helical nanobelts (HNBs). High- and low-doped semiconductor HNBs showed higher swimming performance than the metal (Cr/Ni)-coated HNB and the best performances are achieved with type 4 (dielectric).

in the case of metallic HNB3, the gravitational force can also increase the surface interaction force by dragging it down to the substrate. The detailed calculation and comparison of buoyancy force and gravitational force are not described here; however, the resulting non-fluidic forces (as the difference between the gravitational force and the buoyancy force) on HNB3 is 0.94 pN, which is two times higher than on HNB1 (0.43 pN). These negative effects on HNB3 reduce its swimming performance compared to the others (Figure 9). The result of HNB4 is contrary to HNB3 even though additional layer was deposited onto the surface. This can be explained by the fact that the non-fluidic force of HNB4 was decreased by the increased buoyancy force from the photoresist, which has much lower density than both gold and nickel. The result clearly shows the high dependency on the surface charge and thus the zeta potential in the dielectric surface coating on the HNB compared to conductive or semiconductor materials (Figure 9).

5.2. HNBs with different hydrodynamic frictions

In addition to the increased zeta potential by surface coatings, hydrodynamic friction can be reduced by hydrophobic surface creation. HNBs were divided into two groups. Hydrophobic HNBs were collected in the isopropyl alcohol medium to avoid oxidation. A second group of HNBs were stored in water for 48 hours to allow oxidation to form a hydrophilic surface. Hydrophobic and hydrophilic HNBs from each group were tethered to the tungsten probe, as shown in Figure 1. Both HNBs are oscillated by external an alternating current (AC) electric field in 1 Hz. Then the amplitude was measured to compare the viscous drag due to the hydrodynamic surface friction at the liquid interface. The hydrophobic-treated HNBs were showing much larger amplitude of oscillation compared to the hydrophilic ones (Figure 1 and see Extensions 1(a) and 1(b)). Furthermore, hydrophobic surface-coated HNBs can also maintain their swimming propulsion during many cycles of iterative oscillations. This is considered to be due to the self-cleaning of the hydrophobic surface of HNBs by particles in the liquid medium.

5.3. Demonstrations of other motions

In addition to the unusually high swimming performances of the proposed HNBs driven by electro-osmotic force, various swimming propulsions are also demonstrated, as shown in Figure 10. Passive rotation during their linear propulsion was demonstrated by incorporating the 3D asymmetric shape of the HNBs and increased hydrodynamic surface friction of their surfaces (Figure 10(a) and Extension 4). This passive rotation could be advantageous to reduce the viscous drag during their linear swimming propulsion. Moreover active oscillation by external AC electric field can further reduce the viscous drag as demonstrated in Figure 10(b) (Extension 5). For the demonstration, a tethered HNB on one end to the substrate was oscillated by an external AC electric field at 3 Hz. For certain applications, such as drug delivery in microfluidics, it may be important to manipulate multiple swimmers simultaneously. Figure 10(c) demonstrates the swarm-like swimming behaviors of several HNBs to show their potential possibilities (Extension 6). The collaborative tasks could be more important, depending on the complexity and dimension of the target objects. These various swimming behaviors should further be investigated by combining with other external power sources.

5.4. Comparison with other swimmers

Table 2 summarizes the swimming performances of the microswimmers with helical morphology. Compared to two rotating magnetic propulsions of helical nanostructures, the demonstrated electro-osmotic propulsion of HNBs showed much higher swimming performance in terms of maximum swimming velocity and manipulation force. This can

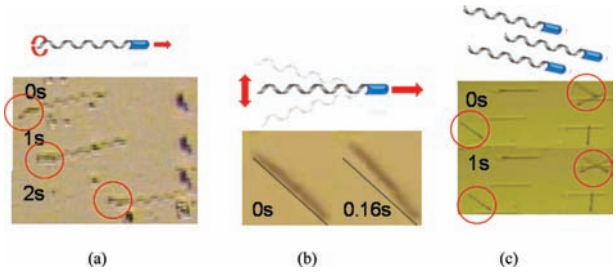

Fig. 10. Various motions of helical nanobelts (HNBs) are demonstrated: (a) passive rotation during the linear swimming propulsion due to the hydrodynamic friction; (b) oscillation motions generated by external alternating current electric field (3 Hz); and (c) swarm-like motion of multiple HNBs.

be explained by the limit of increasing rotating frequency with quite low cut-off frequency at around a few tens of hertz in the case of pure rotating propulsion (Zhang et al., 2009b). It should be noted that the principle of rotating propulsion makes swimmers move only one pitch per each rotation. Therefore, pure rotating propulsion without the aid of a gradient pulling under an electromagnetic field has the principle limit of increasing the swimming performance mainly due to low cut-off frequency. In comparison, electro-osmotic force-based propulsion can show the relatively proportional increase of swimming performance while increasing external field intensity, as shown in Figure 6. Moreover, the passive motions generated at much higher field intensity can overcome the viscous drag, thus further increase the swimming performance exponentially. The demonstrated velocity (1785 μm/s) can reach 90 times faster and the manipulation force can reach around 1.3 nN, which is 1000 times higher than others. Moreover, HNBs can apply a large pressure up to 375.5 Pa, which can be advantageous for local manipulation, such as on biological membranes. Their swimming performance is even comparable to some of nature's bacteria with extremely high motility, as shown in Table 2. Although the demonstrated swimming performance does not reach the one of the MC-1 cell with unusually high motility (Martel et al., 2009a), it exceeds the one of *E. coli* bacteria.

The maximum force of 1.3 nN was estimated when HNBs are propelled by electro-osmotic force at maximum velocity. To estimate the deformation of HNBs due to the applied force, in situ mechanical property characterization was performed using the method shown in Hwang et al. (2009). As a result, the non-linear mechanical property of HNBs was clearly revealed. The large range displacement of the same type and dimension of HNBs due to tensile elongation was measured. The stiffness of HNBs varies from 0.0031 N/m at the neutral position to 0.297 N/m at full elongation. If the HNBs are fixed in one end, they can deform in the longitudinal direction up to 419 nm at 1.3 nN force. This maximum deformation is ignorable compared with the original length of the HNBs (74 μm). Considering that torsional or bending stiffness is much smaller

Table 2. Propulsion performance comparison of helical structures: Mag. 1 (Zhang et al., 2009a,b, 2010); Mag. 2 (Ghosh and Fischer, 2009); EOF (Electro-osmotic flow); *E. coli* (Berg and Brown, 1972; Berg, 2004); MC-1 cells (Martel et al., 2009a)

	Mag. 1	Mag. 2	**EOF**	*E. coli*	MC-1
Length/diameter [μm]	50/2.8	2/0.2	**74/2.1**	2/0.5	2/2
Max. vel. [μm/s]	18	40	**1785**	20	300
Body-length/second	0.4×	20×	**24×**	10×	150×
Force [pN]	3.0	∼1.0	**1300**	0.6	>4
Pressure [Pa]	0.5	31.8	**375.5**	3.1	>1.3
Propulsion motions	Rotation, swarm, pumping by fluid	Rotation, swarm	**Gradient pulling, pumping by EOF, rotation, oscillation, swarm**	Chemotaxy, rotation, swarm	Magnetotaxy, flagella

(around 1/1000 ratio) than the longitudinal stiffness, the force of 1.3 nN can cause much more deformation in the torsional or bending direction during swimming propulsion of untethered HNBs. This can explain the non-continuous swimming propulsion, as shown in Figure 7. This repeated deformation, in combination with the intrinsic piezoelectric surface charge of HNBs created by their repeated mechanical deformations, could further improve the swimming performance of HNBs. For the micromanipulation of HNBs, this slight longitudinal deformation around 419 nm at 1.3 nN should not influence much effect. Even though HNBs swim with much higher force around the micro Newton range, they can survive within their full elongation thanks to their non-linear mechanical property. The maximum tolerable force of HNBs was estimated at full elongation up to 2.95 μN.

The geometry-dependant swimming performances, summarized in Table 2, can further be improved by further size reduction and/or surface coating with dielectric materials. In addition to the propulsion velocity and force, various propulsion motions are also important for different applications. The electro-osmotic propulsion of HNBs demonstrated gradient pulling, jellyfish-like pumping propulsion, flagella-like rotation, shark-like oscillation, and swarm-like swimming behaviors. These various possible motions of the proposed propulsion will reduce viscous drags to allow them to adapt in different swimming environments in liquid medium. The demonstrated characteristics in both propulsion performance and maneuverability are also great features for mobile microscopic swimmers to be able to interact with dynamic physical agents in various biological applications.

5.5. Proposed solutions toward in vivo applications

The absolute voltage applied in this work ranges from a few volts to a few tens of volts and it is over biologically admissible limits in most cases. It is known that the minimum current a human can feel varies from 1 mA of AC at 60 Hz to 5 mA for DC. If the current is higher than 60 mA of AC at 60 Hz or 300–500 mA of DC, it can cause tissue damage or fibrillation leading to cardiac arrest (Berkow, 1997). Therefore, the current estimation is inevitable to predict potential risks prior to any in vivo consideration. We can estimate the current flowing through the isopropyl alcohol or deionized water in the demonstrated experiment to charge the HNBs. The electrical resistance of isopropyl alcohol and deionized water that we used in the experiment is around 5 Mohm. In the maximum voltage applied as 200 V, the current through the liquid is around 40 μA, which is extremely small compared to the potential risk value as described above (300–500 mA of DC). Considering the electrical resistance of healthy blood (550 ohm; Turner, 1902), we can estimate the necessary voltage to be around 22 mV, which is extremely low. This can further be reduced by increasing the zeta potential of the HNB from surface optimization. In this paper, surface coating with dielectric material resulted in increasing the zeta potential. Moreover, the human body is always exposed to high voltages from various sources, such as charged nylon clothes (21 kV), wool clothes (9 kV), and cotton clothes (7 kV).

However, it should be noted here that the experiments are achieved in an open chamber in a Petri dish. It is safe to assume a certain amount of offset voltage compared to the expected behavior in a smaller closed channel. In the case of a closed channel, such as a human blood vessel, the propulsion force can further be enhanced by the reduced gravitational force, thus increasing buoyancy force. Furthermore, the surface interaction from the Petri dish, namely Vans der Waals adhesion, can be minimized as well in the case of the closed-channel experiments. A dedicated microfluidic test chamber mimicking in vivo conditions is actually in the works.

For in vivo biomedical applications of the electro-osmotic HNB swimmers, non-invasive and external electric field generation is inevitable. As one solution, patch-type external embedded electrodes can be considered to control the swimming motions of HNBs remotely. Actuation from the light-driven surface charge creation, not discussed here, could be an alternative solution (Extension 7).

6. Conclusion

The demonstrated direct pulling of HNBs by electro-osmotic pumping was proven to be an efficient energy conversion mechanism for microscopic artificial swimming objects and overcomes easily the viscous drag and gravitational forces in an aqueous environment at low Reynolds numbers. Swimming velocities as fast as 1.8 mm/s (24 times the body length per second), manipulating forces and pressure as high as 1.3 nN and 375.5 Pa, respectively, are achieved by HNBs propelled by an electro-osmotic force under an external electric field. These performances are higher than other state-of-the-art micro-scale artificial swimmers with physical energy conversion. An inertial effect was observed above a critical velocity, and was speculated as the reason why the electro-osmotic HNB swimmers could outrun natural bacteria. Unusual and discontinuous pumping propulsion, such as that found in jellyfish, was observed from high-speed video camera analyses. Hydrodynamic simulation of this unusually fast swimmer revealed a very laminar flow around the HNB with a torque inside it. Although helical morphology with a thin film is beneficial to such fast swimming at low Reynolds numbers, the swimming performance appears to depend highly on the surface conditions. Among the tested four different types, the dielectric polymer-coated HNB showed the best swimming performance compared to others with metallic or semiconductor surfaces. These unusually dynamic swimming performances were attributed to the features of the HNB, with the reduced viscous drag attributed to self-adapting passive motion, the increased zeta potential attributed to piezoelectric self-harvesting energy, and the minimized surface friction attributed to hydrophobicity. These HNBs can be used as wireless liquid manipulators and assemblers for biomedical or micro/nano-electrical mechanical system (MEMS/NEMS) applications or remote physical or chemical detection by functionalizing with proper read outs. For these complex tasks, it would be necessary to improve the control schemes and methods, implemented through finer hydrodynamic finite element model simulations.

Notes

1. Note that the propulsion is considered as the electro-osmotic force applied from the HNB surface to the liquid medium, hence the resulting motion is in the opposite direction

Acknowledgements

We thank the clean room staff of the Laboratoire de Photonique et de Nanostructures (LPN-CNRS) for technical support. We thank Dr Sophie Bouchoule for initiating the contact at LPN under the Recherche Technologique de Base (RTB) network. We also thank Prof Hideki Hashimoto, the University of Tokyo, for allowing us to use their manipulators.

Funding

This work was supported by the French National Agency of Research ANR, through the NANOROL project.

Conflict of interest statement

None declared.

References

Acosta JC, Hwang G, Polesel-Maris J and Régnier S (2011) A tuning fork based wide range mechanical characterization tool with nanorobotic manipulators inside a scanning electron microscope. *Review of Scientific Instruments* 82(3): 035116.

Abbott JJ, Peyer KE, Lagomarsino MC, Zhang L, Dong LX, Kaliakatsos IK, et al. (2009) How should microrobots swim? *International Journal of Robotics Research* 28(11–12): 1434–1447.

Behkam B and Sitti M (2006) Bacterial flagella-based propulsion and on/off motion control of microscale objects. *Applied Physics Letters* 90(2): 023902(1–3).

Bell DJ, Dong LX, Nelson BJ, Golling M, Zhang L and Grutzmacher D (2006) Fabrication and Characterization of three-dimensional InGaAs/GaAs nanosprings. *Nano Letters* 6(4): 725–729.

Bell DJ, Leutenegger S, Hammar KM, Dong LX and Nelson BJ (2007) Flagella-like propulsion for microrobots using a magnetic nanocoil and rotating electromagnetic field. In: *Proceedings of the IEEE International Conference on Robotics and Automation*, pp. 1128–1133.

Berg HC (2004) *E. coli in Motion*. New York: Springer.

Berg HC and Brown DA (1972) Chemotaxis in Escherichia coli analysed by three-dimensional tracking. *Nature* 239(5374): 500–504.

Berkow R (1997) Electrical injuries. In: *The Merck Manual of Medical Information: Home Edition*. New York: Merck.

Chang ST, Beaumont E, Petsev DN and Velev OD (2007b) Remotely powered distributed microfluidic pumps and mixers based on miniature diodes. *Lab on a Chip* 8: 117–124.

Chang ST, Paunov VN, Petsev DN and Velev OD (2007a) Remotely powered self-propelling particles and micropumps based on miniature diodes. *Nature Materials* 6(3): 235–240.

Dreyfus R, Baudry J, Roper ML, Fermigier M, Stone HA and Bibette J (2005) Microscopic artificial swimmers. *Nature* 437(6): 862–865.

Gao PX, Mai W and Wang ZL (2006) Superelasticity and nanofracture mechanics of ZnO Nanohelices. *Nano Letters* 6(11): 2536–2543.

Ghosh A and Fischer P (2009) Controlled propulsion of artificial magnetic nanostructured propellers. *Nano Letters* 9(6): 2243–2245.

Honda T, Arai KI and Ishiyama K (1996) Micro swimming mechanisms propelled by external magnetic fields. *IEEE Transactions on Magnetics* 32(5): 5085–5087.

Hunter RJ (2001) *Foundations of Colloid Science*. New York: Oxford University Press.

Hwang G, Hashimoto H, Bell DJ, Dong LX, Nelson BJ and Schon S (2009) Piezoresistive InGaAs/GaAs nanosprings with metal connectors. *Nano Letters* 9(2): 554–561.

Ishiyama K, Arai KI, Sendoh M and Yamazaki A (2003) Spiral-type micro-machine for medical applications. *Journal of Micromechatronics* 2(1): 77–86.

Kosa G, Jakab P, Hata N, Jolesz F, Neubach Z, Shoham M, et al. (2008) Flagella swimming for medical micro robots: theory, experiments and application. In: *Proceedings of the 2nd IEEE RAS-EMBS International Conference on Biomedical Robotics and Biomechatronics*, pp.258–263.

Laocharoensuk R, Burdick J and Wang J (2008) Carbon-nanotube-induced acceleration of catalytic nanomotors. *ACS Nano* 2(5): 1069–1075.

Little WC, Smith ML, Ebneter U and Vogel V (2008) Assay to mechanically tune and optically probe fibrillar fibronectin conformations from fully relaxed to breakage. *Matrix Biology* 27(5): 451–461.

Martel S, Felfoul O, Mathieu J, Chanu A, Tamaz S, Mohammadi M, et al. (2009b) MRI-based medical nanorobotic platform for the control of magnetic nanoparticles and flagellated bacteria for target interventions in human capillaries. *The International Journal of Robotics Research* 28: 1169–1182.

Martel S, Tremblay C, Ngakeng S and Langlois G (2006) Controlled manipulation and actuation of micro-objects with magnetotactic bacteria. *Applied Physics Letters* 89: 233804–233806

Martel S, Tremblay C, Ngakeng S and Langlois G (2009a) Flagellated magnetotactic bacteria as controlled MRI-trackable propulsion and steering systems for medical nanorobots operating in the human microvasculature. *The International Journal of Robotics Research* 28: 571–582.

Mei YF, Huang G, Solovev AA, Urena EB, Monch IM, Ding F, et al. (2008) Versatile approach for integrative and functionalized tubes by strain engineering of nanomembranes on polymers. *Advanced Materials* 20: 4085–4090.

Park SJ, Goodman MB and Pruitt BL (2007) Analysis of nematode mechanics by piezoresistive displacement clamp. *Proceedings of the National Academy of Sciences of United States of America* 104(44): 17376–17381.

Purcell EM (1977) Life at low Reynolds number. *American Journal of Physics* 45(1): 3–11.

Steager E, Kim CB, Naik C, Patel J, Bith S, Reber L, et al. (2007) Control of microfabricated structures powered by flagellated bacteria using phototaxis. *Applied Physics Letters* 90(26): 263901(1–3).

Sundararajan S, Lammert PE, Zudans AW, Crespi VH and Sen A (2008) Catalytic motors for transport of colloidal cargo. *Nano Letters* 8(5): 1271–1276.

Solovev AA, Mei YF, Urena BE, Huang G and Schmidt OG (2009) Catalytic microtubular jet engines self-propelled by accumulated gas bubbles. *Small* 5(14): 1688.

Turner D (1902) The electrical resistance of the blood. *Nature* 66(1701): 127.

Turner L, Ryu WS and Berg HC (2000) Real-time imaging of fluorescent flagellar filaments. *Journal of Bacteriology* 182(10): 2793–2801.

Varoutsis S, Laurent S, Sagnes I, Lemaitre A, Ferlazzo L, Mériadec C, et al. (2005) Reactive-ion etching of high-Q and submicron-diameter GaAs/AlAs micropillar cavities. *Journal of Vacuum Science & Technology B* 23(6): 2499–2503.

Wang ZL and Song JH (2006) Piezoelectric nanogenerators based on zinc oxide nanowire arrays. *Science* 312: 242–246.

Xu S, Qin Y, Xu C, Wei Y, Yang R and Wang ZL (2010) Self-powered nanowire devices. *Nature Nanotechnology* 5: 366–373.

Zhang L, Abbott JJ, Dong LX, Kratochvil BE, Bell D and Nelson BJ (2009a) Artificial bacteria flagella: fabrication and magnetic control. *Applied Physics Letters* 94(6): 064107(1–3).

Zhang L, Abbott JJ, Dong LX, Peyer KE, Kratochvil BE, Zhang H, et al. (2009b) Characterizing the swimming properties of artificial bacterial flagella. *Nano Letters* 9(10): 3663–3667.

Zhang L, Peyer KE and Nelson BJ (2010) Artificial bacteria flagella for micromanipulation. *Lab on a Chip* 10(17): 2203–2215.

Zhang L, Ruh E, Grutzmacher D, Dong LX, Bell DJ, Nelson BJ, et al. (2005) Controllable fabrication of SiGe/Si and SiGe/Si/Cr helical nanobelts. *Nanotechnology* 16: 655–663.

Appendix: index to multimedia extensions

The multimedia extensions to this article are at: http://www.ijrr.org.

Extension	Type	Description
1	Video	Motions of HNBs with hydrophobic and hydrophilic surfaces
2	Video	A non-tethered HNB steers according to the field gradient
3	Video	Jellyfish-like swimming propulsion revealed by high-speed camera
4	Video	Passive rotation of HNB during the swimming propulsion by direct pulling
5	Video	Oscillation motion of HNB by external AC electric field
6	Video	Swarm-like swimming behavior of motile HNBs
7	Video	Light-driven actuation of HNBs